Envelope-function approximation for nonrectangular $Hg_{1-x}Cd_xTe$ superlattices

K. C. Hass and D. J. Kirill*
Research Staff, Ford Motor Company, P.O. Box 2053, Dearborn, Michigan 48121-2053
(Received 8 March 1990)

The standard eight-band Kane model envelope-function formalism for rectangular superlattices (SL's) is extended to compositionally graded and doping SL's with arbitrary potential profiles. SL band structures along the growth direction are described by a set of coupled differential equations that is easily solved numerically with use of Runge-Kutta methods. A detailed application of this approach to graded $Hg_{1-x}Cd_xTe$ SL's is presented. For a given period and a wide range of band offsets, the SL band gap increases as the composition profile changes from rectangular to sinusoidal to triangular (symmetric) to sawtooth (asymmetric). This and other effects of SL shape are discussed in terms of known quantum-well results and the inherent degree of "interdiffusion" in the SL. Calculated subband structures for $Hg_{1-x}Cd_xTe$ sawtooth SL's agree well with recent tight-binding calculations. An inconsistency in the limited experimental data available for this system is identified.

I. INTRODUCTION

Most realistic electronic-structure calculations for semiconductor superlattices (SL's) assume that the constituent band edges vary in a rectangular manner.[1] Many of the theoretical techniques developed for these calculations are therefore applicable only to undoped compositional superlattices with sharp interfaces (e.g., GaAs/AlAs). The present paper is concerned with an extension of one of these techniques—the multiband envelope-function approximation[1-3] (EFA)—to systems with more complicated band-edge profiles. The approach that we develop is quite general and is intended for applications to both doping SL's and to compositionally graded systems (either intentionally graded or resulting from interdiffusion.) In a previous study,[4] we used this approach to demonstrate the feasibility of developing an 8–12-μm infrared detector based on an $InAs_{1-x}Sb_x$ doping SL. Here we present a more detailed account of this method and consider its application to compositionally graded $Hg_{1-x}Cd_xTe$ SL's of various shapes.

The EFA is widely recognized as one of the most simple and versatile techniques available for studying semiconductor SL's.[1] Single-band EFA ("effective-mass theory") calculations are routinely performed for arbitrary potential shapes and usually provide valuable insight.[5-7] Multiband EFA calculations for rectangular SL's yield more quantitative descriptions that have been successfully compared in many cases to experiments[1,3] and to more sophisticated calculations[8,9] (e.g., tight-binding or pseudopotential). Previous attempts at extending the multiband EFA to nonrectangular SL's have generally had limited applicability and/or involved cumbersome numerical techniques.[10-12] The present approach, by contrast, applies to any direct-band-gap diamond- or zinc-blende-structure SL system and employs standard numerical methods[13] (Runge-Kutta). The basic EFA differential equations that we consider are derived from the modified eight-band Kane model $\mathbf{k}\cdot\mathbf{p}$ Hamiltonian used by Johnson *et al.*[3] Although this Hamiltonian includes only one second-order $\mathbf{k}\cdot\mathbf{p}$ term, it provides an accurate description of the electron (el), light-hole (lh), heavy-hole (hh), and spin-orbit split-off (so) bands in open-gap semiconductors and the corresponding bands in inverted-gap materials (e.g., HgTe). EFA results based on this Hamiltonian for the lowest subbands in rectangular HgTe/CdTe SL's are virtually indistinguishable from those of a 54-band $\mathbf{k}\cdot\mathbf{p}$ model.[14]

To focus the discussion, we consider the application of this approach to the four distinct types of graded $Hg_{1-x}Cd_xTe$ SL's shown in Fig. 1. The actual growth of such structures by laser-assisted molecular-beam epitaxy (MBE) has recently been reported.[11,15,16] Figures 1(a) and 1(b) represent the familiar rectangular SL and a sinusoidal grading, respectively. To be consistent with Ref. 16, we will refer to the symmetric structure in Fig. 1(c) as a triangular SL and the asymmetric structure in Fig. 1(d) as a sawtooth SL.

Preliminary annealing studies[16] suggest that graded $Hg_{1-x}Cd_xTe$ SL's are less sensitive to interdiffusion than rectangular HgTe/CdTe SL's. This result is of considerable technological interest in view of the potential of these materials for infrared applications.[17] The present analysis of graded $Hg_{1-x}Cd_xTe$ SL's is also motivated by the fact that this system provides a highly nontrivial test of the EFA in view of the band crossing that occurs near $x=0.15$. Figure 2 shows the composition dependences (assumed linear[18]) of the Brillouin-zone-center Γ_6, Γ_8, and Γ_7 states in bulk $Hg_{1-x}Cd_xTe$ on an absolute energy scale. At large x, these states represent the conduction-band minimum, the valence-band maximum, and the zone-center spin-order split-off state, respectively, as in most direct-band-gap semiconductors. The inverted-gap structure that occurs for small x results from the crossing of the Γ_6 level below Γ_8. We will assume in this paper that the bulk-band alignments in any of the SL structures shown in Fig. 1 are determined entirely by the composition dependences in Fig. 2. The quantity Λ thus

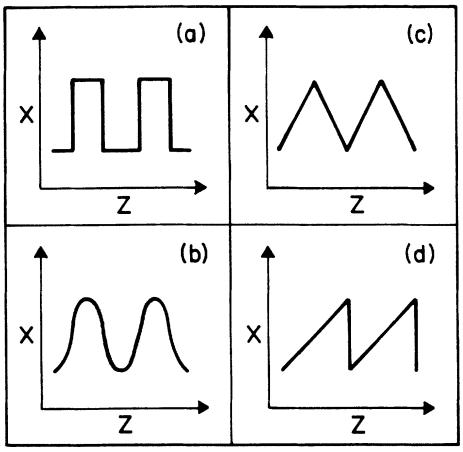

FIG. 1. Schematic profiles of the varying Cd concentrations along the growth directions in $Hg_{1-x}Cd_xTe$ (a) rectangular, (b) sinusoidal, (c) triangular, and (d) sawtooth superlattices.

represents the valence-band offset between HgTe and CdTe, whose value remains controversial,[19] although it is now generally believed[20] to be >300 meV. Because of the band inversion that occurs for small x, the use of a *multiband* EFA approach for $Hg_{1-x}Cd_xTe$ SL's is absolutely essential. The present results for sawtooth SL's are in good agreement with previous tight-binding calculations.[21] A comparison to experiment is less meaningful at this point because of uncertainties in the interpretation of the available data[16] (cf. Sec. III).

II. FORMALISM

We assume that at each position z along the growth direction, the corresponding bulk material is well described by the isotropic eight-band Kane model $\mathbf{k}\cdot\mathbf{p}$ Hamiltonian considered by Johnson *et al.*[3] For a bulk wave vector $\mathbf{k}=(0,0,k_z)$, this Hamiltonian decouples into two equivalent 4×4 blocks, which may be written as

$$\underline{H}(\mathbf{k})=\begin{bmatrix} E_{\rm el}(z) & iP\hbar k_z/m_0 & iP\hbar k_z/\sqrt{2}m_0 & 0 \\ -iP\hbar k_z/m_0 & E_{\rm lh}(z) & 0 & 0 \\ -iP\hbar k_z/\sqrt{2}m_0 & 0 & E_{\rm so}(z) & 0 \\ 0 & 0 & 0 & E_{\rm hh}(z)-\hbar^2k_z^2/2m^*_{\rm hh} \end{bmatrix} . \tag{1}$$

Here the quantities $E_{\rm el}(z)$, $E_{\rm lh}(z)=E_{\rm hh}(z)$, and $E_{\rm so}(z)$ denote the energies of the bulk Γ_6, Γ_8, and Γ_7 states, respectively, at position z (even when Γ_6 lies below Γ_8), P is the bulk momentum matrix element defined in Ref. 3, $m^*_{\rm hh}$ is the heavy-hole effective mass, and m_0 is the free-electron mass. For later convenience, we define the energy units $E_p\equiv3P^2/m_0$. Equation (1) neglects both strain[22] and inversion asymmetry, which are believed to play a minor role in $Hg_{1-x}Cd_xTe$ heterostructures. The inclusion of only one second-order $\mathbf{k}\cdot\mathbf{p}$ term (for the hh band) further simplifies the present approach and is justified by the still rather imprecise knowledge of the $Hg_{1-x}Cd_xTe$ bulk-band structure. In the limit $E_{\rm so}\to\infty$, Eq. (1) reduces to the still simpler "two-band" Hamiltonian (involving coupled el and lh states) used in the original EFA work of Bastard.[2]

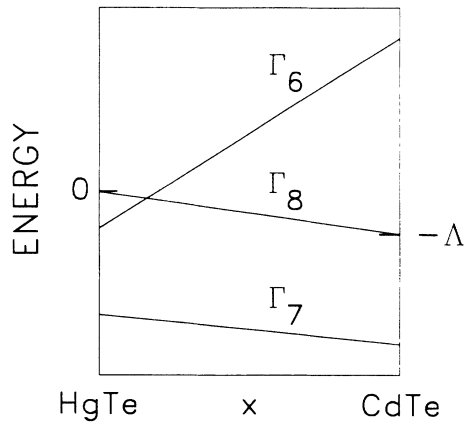

FIG. 2. Assumed composition dependences of the bulk Γ_6, Γ_8, and Γ_7 zone-center states in $Hg_{1-x}Cd_xTe$ from which the superlattice bulk-band-edge profiles are determined. Λ denotes the valence-band offset between HgTe and CdTe.

The SL band structure is most easily calculated in the EFA for SL wave vectors $\mathbf{K}=(0,0,q)$ along the z direction. The dispersion $\perp\hat{\mathbf{z}}$ will not be considered in this paper, but is obtainable from results for $\mathbf{K}=\mathbf{0}$ using the SL $\mathbf{K}\cdot\mathbf{P}$ approach of Johnson *et al.*[3,23] To implement the EFA, we replace the quantity k_z in Eq. (1) by the operator $-i(d/dz)$ and write the wave function for SL band L at wave number q as

$$\Psi_{L,q}(\mathbf{r})=\sum_\alpha F_\alpha^{(L,q)}(z)u_\alpha(\mathbf{r}) , \tag{2}$$

where $u_\alpha(\mathbf{r})$ is the bulk zone-center Bloch function corresponding to the α (=el,lh,so,hh) basis state associated with Eq. (1). As usual, we will assume that the u_α's are independent of x in $Hg_{1-x}Cd_xTe$; it follows that the associated momentum matrix element P is independent of z in the SL. The quantities $F_\alpha^{(L,q)}(z)$ in Eq. (2) are the envelope functions associated with the SL state $\Psi_{L,q}$. According to Bloch's theorem, these quantities must satisfy the condition

$$F_\alpha^{(L,q)}(z+nd)=e^{iqnd}F_\alpha^{(L,q)}(z) , \tag{3}$$

where d is the SL period and n is an integer. Combining the F_α's into a single column vector $\mathbf{F}$ allows us to write the Schrödinger equation for the SL at energy E as

$$\underline{H}(0,\,0,\,-id/dz)\mathbf{F}(z)=E\mathbf{F}(z)\ . \tag{4}$$

Here, and in most of what follows, the superscripts (L,q), which denote a particular SL eigenstate, are suppressed for notational convenience.

The 4×4 matrix equation (4) decouples into a 3×3 matrix equation for the light-particle states (el, lh, and so) and a scalar equation for the hh states. In Hermitian form, the hh equation becomes

$$\frac{\hbar^2}{2}\frac{d}{dz}\left[\frac{1}{m^*_{\rm hh}(z)}\frac{d}{dz}\right]F_{\rm hh}(z)+[E_{\rm hh}(z)-E]F_{\rm hh}(z)=0\ , \tag{5}$$

which is the usual single-band EFA equation[6] for hole states in the presence of a varying band edge $E_{\rm hh}(z)$ and effective mass $m^*_{\rm hh}(z)$. This equation, together with Eq. (3) and the boundary conditions that $F_{\rm hh}$ and $(m^*_{\rm hh})^{-1}dF_{\rm hh}/dz$ must be continuous, completely specify the hh problem in a SL of any shape. The numerical solution of this equation is straightforward using standard Runge-Kutta methods[13] and will not be discussed further. Analytical solutions are also possible in special cases.[5,6]

The 3×3 light-particle equation may be simplified in several ways.[3,7] We first consider a reduction to a single equation for $F_{\rm el}$. This is done by expressing the lh and so rows of Eq. (4) in the form

$$F_{\rm lh}(z)=[E_{\rm lh}(z)-E]^{-1}\left[\frac{\hbar^2E_p}{3m_0}\right]^{-1/2}\frac{dF_{\rm el}}{dz} \tag{6}$$

and

$$F_{\rm so}(z)=[E_{\rm so}(z)-E]^{-1}\left[\frac{\hbar^2E_p}{6m_0}\right]^{-1/2}\frac{dF_{\rm el}}{dz}\ . \tag{7}$$

Substituting Eqs. (6) and (7) back into the first row of Eq. (4) yields the desired equation,

$$\frac{\hbar^2}{m_0}\left[\frac{E_p}{3}\right]\frac{d}{dz}\left[\frac{2}{E-E_{\rm lh}(z)}+\frac{1}{E-E_{\rm so}(z)}\right]\frac{dF_{\rm el}}{dz}+[E-E_{\rm el}(z)]F_{\rm el}(z)=0\ . \tag{8}$$

The associated boundary conditions,[3] obtained by integrating Eq. (8) across a boundary, are that $F_{\rm el}$ and

$$\left[\frac{2}{E-E_{\rm lh}(z)}+\frac{1}{E-E_{\rm so}(z)}\right]\frac{dF_{\rm el}}{dz}$$

must be continuous.

For rectangular SL's, Eq. (8) is sufficient to describe the entire light-particle spectrum provided one avoids the few singular energies corresponding to the $E_{\rm lh}$ or $E_{\rm so}$ values in the different layers. For nonrectangular SL's, however, the singular nature of Eq. (8) poses a more severe problem since the condition $E=E_{\rm lh}(z)$ or $E=E_{\rm so}(z)$ occurs at some z value over a broad range of energies. The most direct way to proceed, for a given energy, is to define internal boundaries at each z value for which one of these conditions is met. Since the true physical solution must be well behaved, the derivative $dF_{\rm el}/dz$ in Eqs. (6) and (7) must vanish at such a boundary. This condition, along with the continuity of $F_{\rm el}$, eliminates the need to integrate directly across a singularity. Numerical difficulties might still arise, however, since Eq. (8) must still be integrated in the vicinity of each singularity.

To circumvent this problem, we employ a more cautious approach that avoids the singular regions entirely. This is made possible by an alternative reduction[3] of the 3×3 light-particle block of Eq. (4) to an equation for $F_{\rm lh}$. In analogy with Eqs. (6)–(8), we obtain the identities

$$F_{\rm so}(z)=\left[\frac{E_{\rm lh}(z)-E}{E_{\rm so}(z)-E}\right]\frac{F_{\rm lh}(z)}{\sqrt{2}} \tag{9}$$

and

$$F_{\rm el}(z)=[E_{\rm el}(z)-E]^{-1}\left[\frac{\hbar^2E_p}{3m_0}\right]^{-1/2}\times\left[\frac{dF_{\rm lh}}{dz}+\frac{1}{2}\frac{d}{dz}\left[\frac{E_{\rm lh}(z)-E}{E_{\rm so}(z)-E}\right]F_{\rm lh}(z)\right]\ , \tag{10}$$

and the associated lh equation,

$$\frac{\hbar^2}{m_0}\left[\frac{E_p}{3}\right]\frac{d}{dz}\left[\frac{1}{E_{\rm el}(z)-E}\frac{d}{dz}\left[\frac{2E_{\rm so}(z)+E_{\rm lh}(z)-3E}{E_{\rm so}(z)-E}\right]\right]\times F_{\rm lh}(z)+[E_{\rm lh}(z)-E]F_{\rm lh}(z)=0\ . \tag{11}$$

It is interesting to note in passing that, in the two-band model of Bastard[2] ($E_{\rm so}\to\infty$), Eq. (11) is identical to Eq. (8) with el and lh interchanged. For finite $E_{\rm so}$, the appropriate boundary conditions corresponding to Eq. (11) are that the quantities

$$\left[\frac{2E_{\rm so}(z)+E_{\rm lh}(z)-3E}{E_{\rm so}(z)-E}\right]F_{\rm lh}(z)$$

and

$$\frac{1}{E_{\rm el}(z)-E}\frac{d}{dz}\left[\frac{2E_{\rm so}(z)+E_{\rm lh}(z)-3E}{E_{\rm so}(z)-E}\right]F_{\rm lh}(z)$$

must be continuous.[3]

The reason for considering this alternative formulation is that, in the vicinity of a z value for which $E=E_{\rm lh}(z)$, which would be a singularity in Eq. (8), Eq. (11) is perfectly well behaved.[24] Conversely, Eq. (8) is well behaved in the vicinity of a z value for which $E=E_{\rm el}(z)$, which would be a singularity in Eq. (11). At an energy that intersects only one bulk band, $E_{\rm el}(z)$ or $E_{\rm lh}(z)$, we therefore consider only whichever equation—(8) or (11)—is nonsingular. Following the heavy-hole procedure, we solve this equation numerically using a Runge-Kutta approach, together with the appropriate boundary conditions and the Bloch condition, Eq. (3). In the more complicated

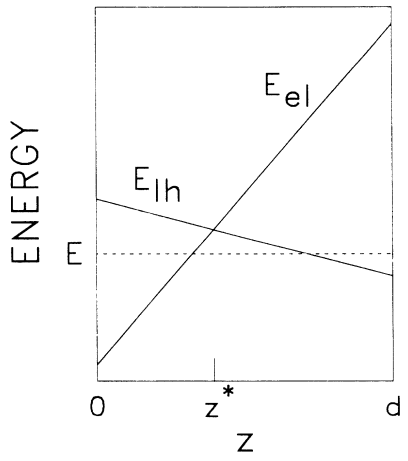

FIG. 3. Example of a sawtooth superlattice of period d with $E_{el}(z)$ and $E_{lh}(z)$ intersecting at the point z^*. To avoid numerical difficulties at the energy E, Eqs. (8) and (11), are solved on the left and right sides of z^*, respectively.

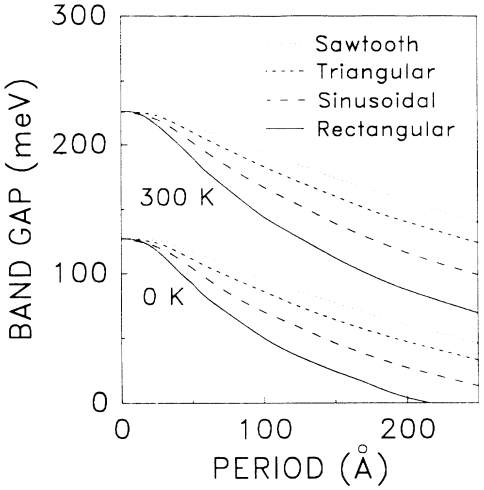

FIG. 4. Calculated band gaps at 0 and 300 K (assuming $\Lambda=350$ meV) as functions of period for the four $Hg_{1-x}Cd_xTe$ superlattices in Fig. 1 with $0.05 \leq x \leq 0.4$. The rectangular superlattices here and in Figs. 5 and 6 have equal layer thicknesses.

case of an energy that intersects both $E_{el}(z)$ and $E_{lh}(z)$, we first divide the interval of interest up at the point z^*, which is defined by the condition that $E_{el}(z^*)=E_{lh}(z^*)$ (cf. Fig. 3). We then obtain numerical solutions over the entire interval by applying the Runge-Kutta method to Eqs. (8) and (11) on opposite sides of z^* in a manner that avoids the singularities [e.g., Eq. (8) would be used to the left of z^* in Fig. 3]. The full boundary-value problem is then easily solved by invoking the SL boundary and Bloch conditions along with the additional requirements that $F_{el}(z)$ and $F_{lh}(z)$ must be continuous at z^*.

III. APPLICATION TO $Hg_{1-x}Cd_xTe$ SUPERLATTICES

Calculations for $Hg_{1-x}Cd_xTe$ SL's are performed using the bulk $\mathbf{k}\cdot\mathbf{p}$ parameters listed in Table I. All except for E_{el} are assumed to be temperature independent and to vary linearly between the HgTe and CdTe parameters of Ref. 3. (The lack of x dependence in E_p and m^*_{hh} follows from this assumption.) As in previous studies,[25] we model temperature effects in the SL by changing the input values of E_{el} in accordance with the known temperature dependence of the bulk-band gap. Unless otherwise specified, we assume the currently most popular value[20] of the valence-band offset between HgTe and CdTe: $\Lambda=350$ meV.

Figure 4 shows the resulting band gaps at 0 and 300 K for the four differently shaped $Hg_{1-x}Cd_xTe$ SL's in Fig. 1. The minimum and maximum x values in each case were chosen to be 0.05 and 0.4, respectively, as in the MBE-grown samples of Ref. 16. For the sake of comparison, we constrain the rectangular SL's here to have individual layer thicknesses equal to half their periods. This fixes the average Cd concentration in each SL considered to be $\bar{x}=0.225$. An immediate consequence of this is that all of the SL gaps at a given temperature converge in the limit of small period to the gap of the corresponding alloy with $x=0.225$. This behavior is well known[26] in the case of rectangular SL's and is intuitively reasonable for the other shapes as well. With increasing period, all of the SL gaps decrease monotonically at a rate that increases from sawtooth to triangular to sinusoidal to rectangular. The rate of decrease is independent of temperature in the sawtooth case, but the variation among the results for different shapes is slightly larger at 300 K than at 0 K.

The observed shape dependence is consistent with the known effects of interdiffusion in HgTe/CdTe SL's.[27,28] For a given period, the least "interdiffused" structure, the rectangular SL, has the smallest band gap, while the most "interdiffused" structure, the sawtooth SL, has the largest gap, closest to that of the completely mixed alloy. The relative ordering of SL gaps is also consistent with simple quantization conditions[7,16] for differently shaped quantum wells (QW's). The lowest-energy levels in rectangular and sawtooth QW's, for example, fall off as L^{-2} and $L^{-2/3}$, respectively, where L is the well width.[16] Al-

TABLE I. Bulk $\mathbf{k}\cdot\mathbf{p}$ parameters for $Hg_{1-x}Cd_xTe$ used as input for superlattice calculations. All quantities other than E_{el} are assumed independent of temperature. All energies in eV; m^*_{hh} in units of the free-electron mass m_0.

E_p	m^*_{hh}	E_{so}	$E_{lh,hh}$	E_{el}(0 K)	E_{el}(300 K)
17.5	0.7	$-1.0+(0.1-\Lambda)x$	$-\Lambda x$	$-0.3+(1.9-\Lambda)x$	$-0.122+(1.547-\Lambda)x$

though useful as a heuristic device, this QW analogy may not always be reliable in the case of $Hg_{1-x}Cd_xTe$ SL's because of their complicated "type III" (i.e., inverted-gap) nature.

Qualitatively, the present results reproduce many of the features seen in the limited optical-absorption data of Cheung and Chen.[16] In particular, Fig. 4 confirms the reduced sensitivity of the SL band gap to the period in a graded system. It was this effect led Cheung and Chen to suggest that, for a given band gap, a $Hg_{1-x}Cd_xTe$ sawtooth SL might be less sensitive to interdiffusion than the corresponding rectangular SL.

A closer examination of the experimental data, however, reveals what we believe is an internal inconsistency in Ref. 16; in several cases, the "fundamental" SL gap reported is significantly larger than that of the equivalent bulk alloy (same $\bar{x}$) at the same temperature. For example, a 125-Å-period sawtooth SL with $\bar{x}=0.225$ is claimed to have a gap of close to 300 meV at 300 K, while the alloy gap at that temperature is only 226 meV. Without this warning sign, we would be tempted to attribute the *uniformly* larger experimental gaps (compared to the calculated values) to either a greater amount of interdiffusion or a smaller band offset (cf. Fig. 5) in the MBE-grown samples.[29] While these effects may indeed play a role, they alone cannot account for the observation of SL gaps larger than those of the equivalent alloy. We thus suspect that some of the absorption features that Cheung and Chen[16] identify as fundamental gaps may actually involve higher subband excitations, with the weaker absorption in the gap regions obscured by interference and other effects. An example of such a reinterpretation is given below. Clearly, a more extensive, quantitative, study of optical absorption in graded $Hg_{1-x}Cd_xTe$ SL's would be useful.

The sensitivity of the present results to the value of the band offset is examined in Fig. 5. Calculated gaps at 0 K are plotted over the range $0 \le \Lambda \le 500$ meV for SL's with a fixed period of 125 Å and the same minimum and maximum Cd concentrations as in Fig. 4. The relative ordering of the gaps is unaffected by variations in Λ. The observed reduction in gaps with increasing Λ is well known in the case of rectangular HgTe/CdTe SL's.[20] The magnitude of the reduction from $\Lambda=0$ to $\Lambda=500$ meV itself decreases by more than 50% as the SL shape changes from rectangular to sinusoidal to triangular to sawtooth. This trend is again consistent with a decreasing amount of "interdiffusion" in this series since, in the limit of a completely mixed alloy, the band gap becomes independent of Λ. A decreasing sensitivity to Λ also occurs for any SL shape as the SL period is reduced. Since reasonable changes in Λ produce only quantitative changes in the present results, we will continue to use a fixed offset of 350 meV from here on.

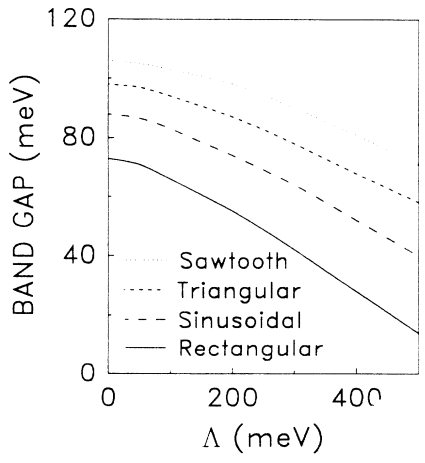

FIG. 5. Sensitivities of the calculated 0-K band gaps to the assumed value of the HgTe/CdTe valence-band offset Λ. The period in each superlattice is 125 Å and the composition range is the same as in Fig. 4.

All of the SL band gaps in Figs. 4 and 5 occur between the lowest SL conduction-band state and the highest SL heavy-hole state. SL subband structures over a more extended energy rate at 0 K are plotted in Fig. 6 for the same composition (a) sawtooth, (b) triangular, and (c) rectangular SL's as discussed above. The solid black and cross-hatched regions in the figure represent the allowed SL heavy-hole and light-particle states, respectively, for $\mathbf{K}=(0,0,q)$. By convention, the three conduction subbands shown for each system are usually denoted $C1$, $C2$, and $C3$, counting upwards in energy, and the three heavy-hole (light-hole) subbands are denoted HH1 (LH1), HH2 (LH2), and HH3 (LH3), counting downwards in energy. For each of these sets of states, the subband edges closest to the fundamental gap lie at $q=0$ for odd-numbered subbands and at $q=\pi/d$ for even-numbered subbands.

A strong similarity exists between Fig. 6(a) and the recent tight-binding results of Chang *et al.*[21] for a $Hg_{1-x}Cd_xTe$ sawtooth system with $0.08 \le x \le 0.45$. Additional EFA calculations (not shown) confirm that the small differences between these two sets of results are due almost entirely to the slightly different composition ranges considered. This consistency between these two theories is similar to that which is regularly achieved for rectangular HgTe/CdTe SL's.[8] The fact that in that case the theories also agree well with experiment[3] further supports our contention that existing data for graded $Hg_{1-x}Cd_xTe$ SL's should be reevaluated. We have already speculated that at least some of the so-called absorption "edges" in Ref. 16 might actually represent higher-energy transitions between SL subbands. To pursue this point, we consider, as an example, the case of the 125-Å-period sawtooth SL for which structure is seen in optical-absorption data[16] near both 300 and 500 meV. In a sawtooth system, all intersubband transitions are allowed even at $\mathbf{K}=\mathbf{0}$ because of the lack of reflection symmetry in the z direction. Figure 6(a) thus suggests that the observed absorption features for a period of 125 Å may be due to HH1 (or HH2)$\rightarrow C2$ and HH3$\rightarrow C3$ transitions, respectively. A more definitive identification is not possible at this point without more quantitative absorption data and a full calculation of the absorption coefficient.

The differences between the subband structures in Fig. 6 for the different SL shapes are best understood by con-

sidering the HH, LH and C states separately. The HH states in each case are extremely narrow even for SL periods as small as 100 Å. This is a consequence of the relatively large m^*_{hh} values in bulk $Hg_{1-x}Cd_xTe$ (cf. Table I), which make it difficult for heavy holes to tunnel through the valence-band-potential barrier, which extends from -17.5 meV ($x=0.05$) to -140 meV ($x=0.4$). We recall that the HH states are described by a decoupled single-band equation, (5), for which the effects of SL shape are well known. The QW analogy should certainly hold in this case. Indeed, we find that, in the limit of large periods, the confinement energies of the lowest HH states in Fig. 6 approach the expected values[7,16,30] for the corresponding QW's. This explains why the separation between successive HH subbands increases in the case of rectangular SL's (where QW energies go as n^2) and decreases in the case of sawtooth and triangular SL's (where QW energies go roughly as $n^{2/3}$). The fact that the separation between HH1 and HH2 is actually larger in the triangular case than in the sawtooth case is also consistent with exact QW results.[16,30] (We note that the differences between the sawtooth and triangular cases are especially interesting since the widths of the classically allowed regions at any energy in these two cases are identical.)

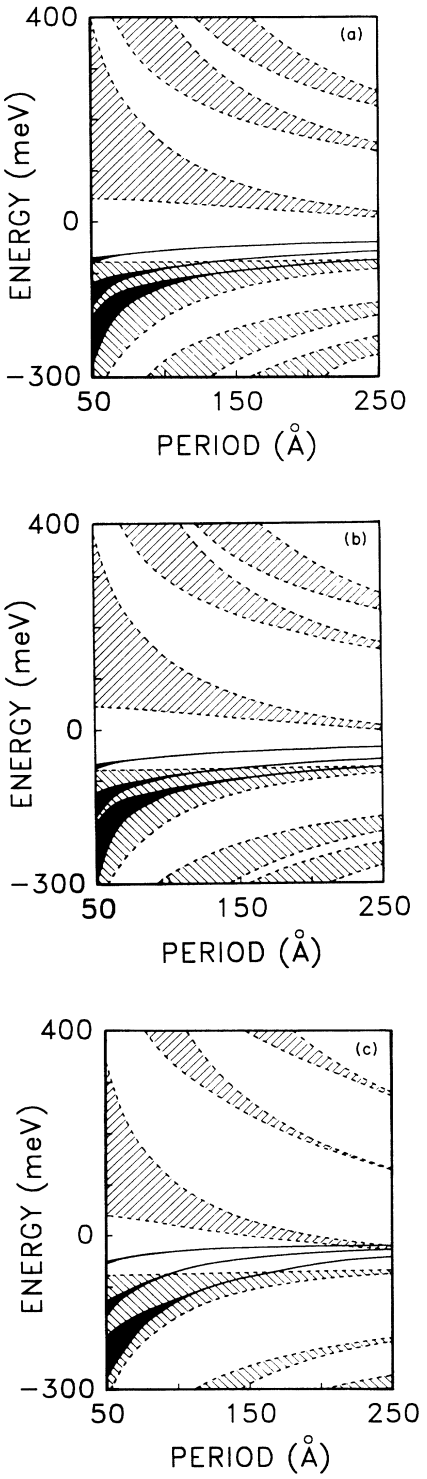

FIG. 6. Theoretical heavy-hole (shaded) and light-particle (cross-hatched) subbands at 0 K, for wave vectors along the growth directions, for the same (a) sawtooth, (b) triangular, and (c) rectangular superlattices as in Fig. 4.

Unlike the HH subbands, whose energies are strongly dependent on the SL shape and period, the upper edges of the LH1 subbands in Fig. 6 appear to be independent of both. The fixed location of these states near -80 meV corresponds to the average energy of the bulk valence-band maximum in these systems. Similar behavior for the uppermost LH1 edge was observed in previous calculations for $InAs_{1-x}Sb_x$ doping SL's.[4] We attribute this effect to the fact that the valence-band-potential barrier in these cases is too small to effectively confine light particles (bulk light-hole effective masses here are $\lesssim 0.04m_0$); the LH1 state thus spreads out and "experiences" the average potential. The detailed behavior of other LH states is more difficult to analyze in view of the considerable band mixing that occurs in $Hg_{1-x}Cd_xTe$ and the inadequacy of the QW analogy for extended states. Nevertheless, some remnants of the QW behavior still exist, such as the larger separation between LH1 and LH2 for the triangular SL, compared to the sawtooth.

Lastly, we turn to the conduction-subband structure. The bulk Γ_6 level in these SL's varies from -223 to $+320$ meV. The SL C states, which are derived primarily from bulk "el" basis functions, are thus more strongly confined than the LH states, despite the approximate equality between bulk electron and light-hole effective masses in $Hg_{1-x}Cd_xTe$. This stronger confinement is reflected in the larger variation in the location of the $C1$ subband minimum with SL shape and period, and in the slightly smaller widths of the $C1$ subbands compared to their LH1 counterparts. As the SL period decreases, the confinement becomes less effective and the $C1$ subband minima all approach the average value of the bulk conduction-band edge, $+49$ meV. The behavior of higher conduction subbands in Fig. 6 is again complicated by the multiband nature of the problem. As was the case for LH subbands, we see a larger separation between $C1$ and $C2$ in the triangular SL, compared to the sawtooth. The rectangular results in Fig. 6(c) are unusual in that the subband width actually decreases from $C1$ to $C2$, but then increases again for $C3$. This is due to the nonmonotonic energy dependence of the tunneling proba-

bility of light-particle states through the $Hg_{0.6}Cd_{0.4}Te$ barrier layers.[23] The same effect does not show up in the sawtooth and triangular SL's because the barrier width itself changes with energy.

To conclude this paper, we consider a more useful comparison of $Hg_{1-x}Cd_xTe$ sawtooth and rectangular SL's from a practical viewpoint. For infrared applications, there is little reason (in theory, at least) to consider any rectangular SL other than that composed of alternating HgTe and CdTe layers.[17] This is the system that any nonrectangular $Hg_{1-x}Cd_xTe$ SL has to compete with. Figure 7 thus compares the 0-K band gaps in two rectangular HgTe/CdTe systems with different ratios of layer thicknesses (1:1 and 3:1) to the 0-K band gaps in two sawtooth systems with equivalent $\bar{x}$ values (0.5 and 0.25). As in Fig. 4, we see a convergence in the limit of small periods to the gaps of the equivalent alloys. The divergence between sawtooth and rectangular results at larger periods is now much larger, however, because of the wider composition ranges (and, hence, larger potential barriers) considered. Because of this divergence, the same 10-μm ($\sim$120-meV) gap that is obtained in a (24 Å HgTe)/(8 Å (CdTe) SL or a (50 Å HgTe)/50 Å CdTe) SL can also be obtained with the much larger periods of 100 and >300 Å, respectively, in the corresponding sawtooth systems.

A comparison of the two 100-Å-period SL's with the same 10-μm gap is particularly interesting. By differentiating the calculated $C1$ dispersion curves, we find that the sawtooth SL, because of its smaller $\bar{x}$ value, has a much smaller electron effective mass ($0.004m_0$ compared to $0.092m_0$). Probability densities associated with the band-edge envelope functions in the two cases are shown in Fig. 8. The larger barrier heights in the rectangular SL result in a stronger localization of both the HH1- and $C1$-edge states. The sharper interfaces in this system also introduce a larger lh component in the $C1$ edge. This latter effect results in a weaker band-edge optical-absorption strength in the rectangular SL. Following Refs. 3 and 4, we find that, for light incident along the z direction, the ratio of the square of the SL band-edge optical matrix element to the square of the bulk hh$\rightarrow$el band-edge matrix element is given by $|\alpha_{vc}|^2$, where

$$\alpha_{vc}=d^{-1}\int_0^d [F_{el}^{C1}(z)]^* F_{hh}^{HH1}(z)dz \ . \tag{12}$$

For the two systems in Fig. 8, the calculated $|\alpha_{vc}|^2$ turns out to be 0.45 for the rectangular SL and 0.61 for the sawtooth SL. This suggests that, given a rectangular SL of a particular period and band gap, it should be possible to construct a *larger-period* sawtooth SL with the same

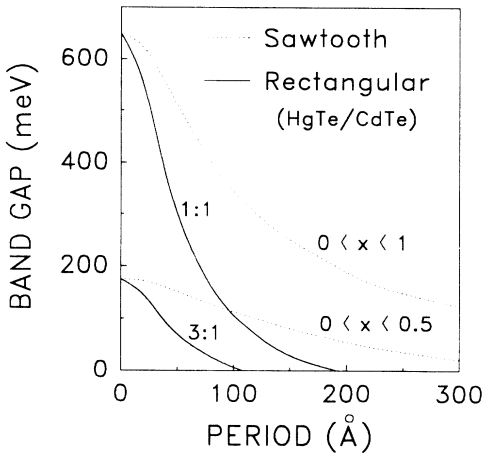

FIG. 7. Comparison of the calculated 0-K band gaps in two HgTe/CdTe rectangular superlattices (with the indicated ratios of layer thicknesses) and two $Hg_{1-x}Cd_xTe$ sawtooth superlattices (with the indicated composition ranges) with the same average Cd concentrations.

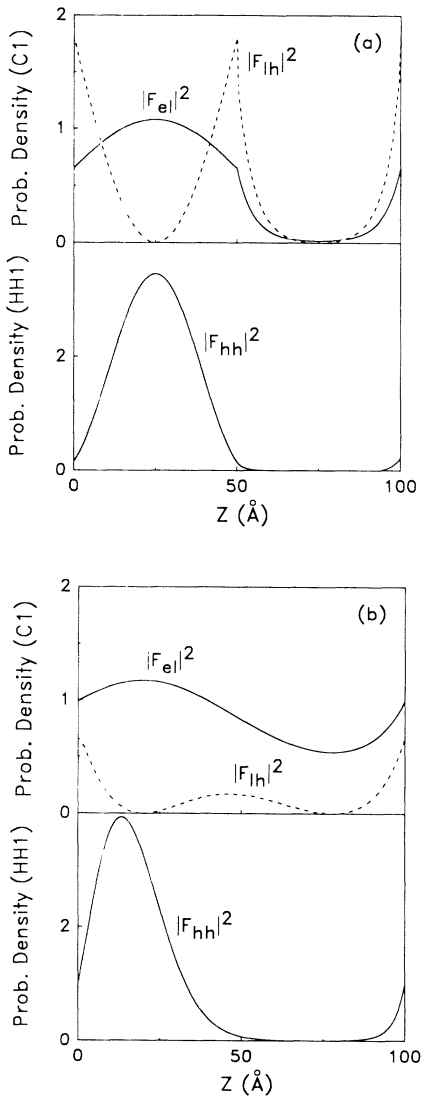

FIG. 8. Calculated probability densities associated with the dominant envelope function contributions to the lowest $C1$ (top) and highest HH1 (bottom) states in (a) a (50 Å HgTe)/(50 Å CdTe) superlattice, and (b) a 100-Å-period sawtooth superlattice with $0 \le x \le 0.5$. A full period is shown in each case, with the Cd concentration increasing from left to right.

gap and a comparable, or even larger, band-edge absorption strength. In view of this result and the possibly enhanced stability of the latter system,[16] further studies of $Hg_{1-x}Cd_xTe$ sawtooth SL's are clearly warranted.

ACKNOWLEDGMENTS

We are grateful to N. F. Johnson for extensive discussions concerning the EFA approach to SL's.

*Present address: Lloyd House, California Institute of Technology, Pasadena, CA 91126.

[1]G. Bastard, C. Delalande, Y. Guldner, and P. Voisin, Adv. Electron. Electron Phys. **72**, 1 (1988), and references therein.

[2]G. Bastard, Phys. Rev. B **25**, 7584 (1982).

[3]N. F. Johnson, H. Ehrenreich, P. M. Hui, and P. M. Young, Phys. Rev. B **41**, 3655 (1990).

[4]K. C. Hass and D. J. Kirill, J. Appl. Phys. (to be published).

[5]J. A. Brum, P. Voisin, and G. Bastard, Phys. Rev. B **33**, 1063 (1986).

[6]V. Milanović, Z. Ikonić and D. Tjapkin, Phys. Rev. B **36**, 8155 (1987).

[7]P. Yuh and K. L. Wong, Phys. Rev. B **38**, 13 307 (1988).

[8]Y.-C. Chang, J. N. Schulman, G. Bastard, Y. Guldner, and M. Voos, Phys. Rev. B **31**, 2557 (1985).

[9]R. Eppenga, M. F. H. Schuurmans, and S. Colak, Phys. Rev. B **36**, 1554 (1987).

[10]A. Fasolini and M. Alterelli, Surf. Sci. **170**, 606 (1986).

[11]Z. Yang, M. Dobrowolska, H. Luo, J. K. Furdyna, J. T. Cheung, and N. Otsuka, Appl. Phys. Lett. **55**, 380 (1989).

[12]K. J. Duff and K. C. Hass, Surf. Sci. **228**, 479 (1990).

[13]W. H. Press, B. P. Flannery, S. A. Teukolsky, and W. T. Vetterling, *Numerical Recipes* (Cambridge University Press, Cambridge, 1986).

[14]N. F. Johnson, H. Ehrenreich, G. Y. Wu, and T. C. McGill, Phys. Rev. B **38**, 13 095 (1988).

[15]J. T. Cheung, E.-H. Cirlin, and N. Otsuka, Appl. Phys. Lett. **53**, 310 (1988).

[16]J. T. Cheung and J.-S. Chen, Appl. Phys. Lett. **53**, 2191 (1988).

[17]D. L. Smith, T. C. McGill, and J. N. Schulman, Appl. Phys. Lett. **43**, 180 (1983).

[18]The coherent-potential-approximation calculations of K. C. Hass, B. Velický and H. Ehrenreich [Phys. Rev. B **27**, 1088 (1983)] support the present assumption that, near the band edges, the electronic structure of $Hg_{1-x}Cd_xTe$ is essentially virtual-crystal-like.

[19]J. Tersoff, Phys. Rev. B **40**, 10 615 (1989), and references therein.

[20]N. F. Johnson, P. M. Hui, and H. Ehrenreich, Phys. Rev. Lett. **61**, 1993 (1988).

[21]Y.-C. Chang, J. Cheung, A. Chiou, and M. Khoshnevisan, J. Appl. Phys. **66**, 829 (1989).

[22]G. Y. Wu and T. C. McGill, Appl. Phys. Lett. **47**, 634 (1985).

[23]N. F. Johnson, H. Ehrenreich, K. C. Hass, and T. C. McGill, Phys. Rev. Lett. **59**, 2352 (1987).

[24]We will only consider the case here for which $E > E_{so}(z)$ for all z. The generalization to avoid a crossing of the E_{so} band as well is straightforward.

[25]J. Reno, I. K. Sou, J. P. Faurie, J. M. Berroir, Y. Guldner, and J. P. Vieren, Appl. Phys. Lett. **46**, 106 (1986).

[26]J. N. Schulman and T. C. McGill, Appl. Phys. Lett. **34**, 663 (1979).

[27]J. N. Schulman and Y.-C. Chang, Appl. Phys. Lett. **46**, 571 (1985).

[28]D. J. Leopold, J. G. Broerman, D. J. Peterman, and M. L. Wroge, Appl. Phys. Lett. **52**, 969 (1988).

[29]We note that in Ref. 11 the observed band gap in a 312-Å-period sinusoidal $Hg_{1-x}Cd_xTe$ SL with $0.05 \leq x \leq 0.45$ is also larger than that predicted theoretically for $\Lambda = 350$ meV. Our calculated results for this system confirm this discrepancy. We strongly suspect that the actual composition profiles in all of the graded $Hg_{1-x}Cd_xTe$ SL's grown to date deviate significantly from what was intended.

[30]T. Ando, A. B. Fowler, and F. Stern, Rev. Mod. Phys. **54**, 437 (1982).